
DESIGN OF SUPERVISION-SCALABLE LEARNING SYSTEMS: METHODOLOGY AND PERFORMANCE BENCHMARKING

A PREPRINT

Yijing Yang

University of Southern California
Los Angeles, California, USA
yijingya@usc.edu

Hongyu Fu

University of Southern California
Los Angeles, California, USA
hongyufu@usc.edu

C.-C. Jay Kuo

University of Southern California
Los Angeles, California, USA
cckuo@sipi.usc.edu

August 18, 2022

ABSTRACT

The design of robust learning systems that offer stable performance under a wide range of supervision degrees is investigated in this work. We choose the image classification problem as an illustrative example and focus on the design of modularized systems that consist of three learning modules: representation learning, feature learning and decision learning. We discuss ways to adjust each module so that the design is robust with respect to different training sample numbers. Based on these ideas, we propose two families of learning systems. One adopts the classical histogram of oriented gradients (HOG) features while the other uses successive-subspace-learning (SSL) features. We test their performance against LeNet-5, which is an end-to-end optimized neural network, for MNIST and Fashion-MNIST datasets. The number of training samples per image class goes from the extremely weak supervision condition (i.e., 1 labeled sample per class) to the strong supervision condition (i.e., 4096 labeled sample per class) with gradual transition in between (i.e., 2^n , $n = 0, 1, \dots, 12$). Experimental results show that the two families of modularized learning systems have more robust performance than LeNet-5. They both outperform LeNet-5 by a large margin for small n and have performance comparable with that of LeNet-5 for large n .

1 Introduction

Supervised learning is the main stream in pattern recognition, computer vision and natural language processing nowadays due to the great success of deep learning. On one hand, the performance of a learning system should improve as the number of training samples increases. On the other hand, some learning systems may benefit more than others from a large number of training samples. For example, deep neural networks (DNNs) often work better than classical learning systems that contain feature extraction and classification two stages. How the quantity of labeled samples affects the performance of learning systems is an important question in the data-driven era. Is it possible to design a supervision-scalable learning system? We attempt to shed light on these questions by choosing the image classification problem as an illustrative example in this work.

Strong supervision is costly in practice since data labeling demands a lot of time and resource. Besides, it is unlikely to collect and label desired training samples in all possible scenarios. Even with a huge amount of labeled data in place, it may still be substantially less than the need. Weak supervision can appear in different forms, e.g., inexact supervision, inaccurate supervision, and incomplete supervision. Labels are provided at the coarse grain (instead of the instance level) in inexact supervision. One example is multi-instance learning [1, 2]. For inaccurate supervision, labels provided may suffer from labeling errors, leading to the noisy label problem in supervised learning [3, 4]. Only a limited number of labeled data is available to the training process in incomplete supervision [5, 6]. Here, we consider the scenario of incomplete supervision.

To improve learning performance under incomplete supervision, solutions such as semi-supervised learning and active learning have been developed. In semi-supervised learning, both labeled and unlabeled data are utilized to achieve better performance [7, 8, 9]. It is built upon several assumptions such as smoothness, low-density, and manifold assumptions

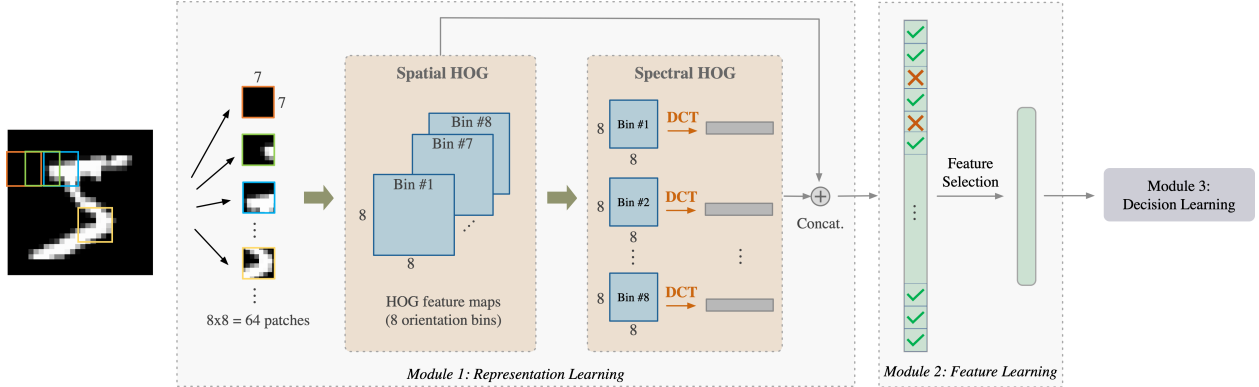


Figure 1: An overview of the HOG-based learning system, where the input image is of size 28×28 .

[10]. In active learning, it attempts to expand the labeled data set by identifying important unlabeled instances that help boost the learning performance most [11, 12]. Another related technology is few-shot learning (FSL) [13] that learns from a very limited number of labeled data without the help of unlabeled data. For example, a N -way- K -shot classification refers to a labeled set with K samples from each of the N classes. Meta learning is often used to solve the FSL problem [14, 15].

Humans can learn effectively in a weakly supervised setting. In contrast, deep learning networks often need more labeled data to achieve good performance. What makes weak supervision and strong supervision different? There is little study on the design of supervision-scalable learning systems. In this work, we show the design of two learning systems that demonstrate an excellent scalable performance with respect to various supervision degrees. The first one adopts the classical histogram of oriented gradients (HOG) [16] features while the second one uses successive-subspace-learning (SSL) features. We discuss ways to adjust each module so that their design is more robust against the number of training samples. To illustrate their robust performance, we compare with the performance of LeNet-5, which is an end-to-end optimized neural network, for MNIST and Fashion-MNIST datasets. The number of training samples per image class goes from the extremely weak supervision condition (i.e., 1 labeled sample per class) to the strong supervision condition (i.e., 4096 labeled sample per class) with gradual transition in between (i.e., 2^n , $n = 0, 1, \dots, 12$). Experimental results show that the two families of modularized learning systems have more robust performance than LeNet-5. They both outperform LeNet-5 by a large margin for small n and have performance comparable with that of LeNet-5 for large n .

The rest of the paper is organized as follows. The design of HOG-based learning systems is examined in Sec. 2, where two methods, called HOG-I and HOG-II, are proposed. The design of SSL-based learning systems is investigated in Sec. 3, where two methods, called IPHop-I and IPHop-II, are presented. Performance benchmarking of HOG-I, HOG-II, IPHop-I, IPHop-II and LeNet-5 is conducted in Sec. 4. Discussion on experimental results is given in Sec. 5. Finally, concluding remarks and future work are given in Sec. 6.

2 Design of Learning Systems with HOG Features

Classical pattern recognition methods consist of feature extraction and classification two steps. One well known feature extraction method is the Histogram of Oriented Gradients (HOG) [16]. Before the big data era, most datasets are small in terms of the numbers of training samples and test samples. As a result, HOG-based solutions are typically applied to small datasets. To make HOG-based solutions scalable to larger datasets, some modifications have to be made. In this section, we propose two HOG-based learning systems, HOG-I and HOG-II. They are suitable for small and large training sizes, respectively.

2.1 Design of Three Modular Components

As mentioned earlier, we focus on the design of a modularized system that can be decomposed into representation learning, feature learning and decision learning three modules. We will examine them one by one below.

2.1.1 Representation Learning

HOG was originally proposed for human detection in [16]. It measures the oriented gradient distribution in different orientation bins evenly spaced over 360 degrees at each local region of the input image. Modifications are made to make

the HOG representation more powerful for multi-class recognition. Images in the MNIST and the Fashion-MNIST datasets have resolution of 28×28 without padding. The proposed HOG representation scheme for them is illustrated in Fig. 1. As shown in the figure, both spatial and spectral HOG representations are considered. Hyper-parameters used in the experiments are specified below.

First, we decompose an input image into 7×7 overlapping patches with stride 3, leading to $8 \times 8 = 64$ patches. HOG is computed within each patch and the number of orientation bins is set to 8. For each orientation bin, there are 8×8 responses in the spatial domain. Thus, each image has a 512-D spatial HOG representation vector. It is called the spatial HOG representation since each element in the vector captures the probability of a certain oriented gradient in a local region. Next, for each bin, we apply the 2D discrete cosine transform (DCT) to 8×8 spatial responses to derive the spectral representation. The DCT converts 64 spatial responses to 64 spectral responses. It is called the spectral HOG representation. Each image has a 512-D spectral HOG representation vector, too. We combine spatial and spectral HOG representations to yield a vector of 1024 dimensions as the joint spatial/spectral HOG features.

2.1.2 Feature Learning

The size of HOG feature set from Module 1 is large. It is desired to select discriminant features to reduce the feature dimension before classification. We adopt two feature selection methods in Module 2 as elaborated below.

When the training size is small, we may consider unsupervised feature selection. One common method is to use the variance of a feature. Intuitively speaking, if one feature has a smaller variance value among all training samples, it is not able to separate different classes well as compared with features that have higher variance values. Thus, we can rank order features from the largest to the smallest variance values and use a threshold to select those of larger variance.

When the training size becomes larger, we can exploit class labels for better feature selection. The advantage of semi-supervised feature selection over unsupervised becomes more obvious as the supervision level increases. Here, we adopt a newly developed method, called Discriminant Feature Test (DFT) [17], for semi-supervised feature selection. DFT computes the discriminant power of each 1D feature by partitioning its range into two non-overlapping intervals and searching for the optimal partitioning point that minimizes the weighted entropy loss. Mathematically, we have the entropy function of the left interval as

$$H_{L,t}^i = - \sum_{c=1}^C p_{L,c}^i \log(p_{L,c}^i), \quad (1)$$

where $p_{L,c}^i$ is the probability of class c in the left interval of the i th feature and t is a threshold. Similarly, we can compute entropy $H_{R,t}^i$ for the right interval. Then, the entropy of the whole range is the weighted average of $H_{L,t}^i$ and $H_{R,t}^i$, denoted by H_t^i . Then, the optimized entropy H_{op}^i for the i th feature is given by

$$H_{op}^i = \min_{t \in T} H_t^i, \quad (2)$$

where T indicates a set of discrete partition points. The lower the weighted entropy, the higher the discriminant power. Top K features with the lowest DFT loss are selected as discriminant features. In our experiments, we select $K = 400$ features out of the 1024 joint spatial/spectral HOG features for MNIST while setting $K = 600$ for Fashion-MNIST.

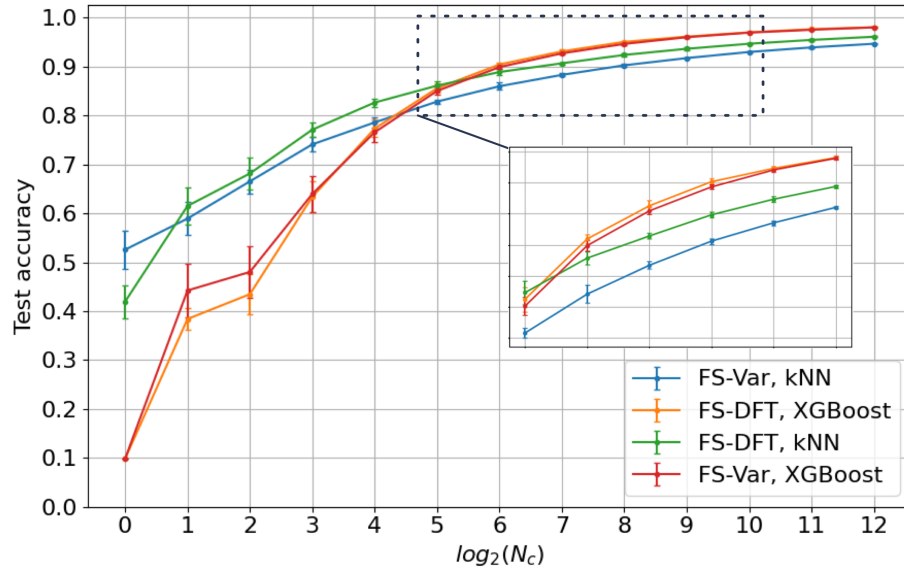
2.1.3 Decision Learning

We consider two classifiers - the k-nearest-neighbor (KNN) classifier and the eXtreme Gradient Boosting (XGBoost [18]) classifier. In a weakly supervised setting with a small number of training samples, the choice is very limited and the distance-based classifier seems to be a reasonable choice. When the training sample becomes larger, we can use more powerful supervised classifier to yield better classification performance. The XGBoost classifier is a representative one.

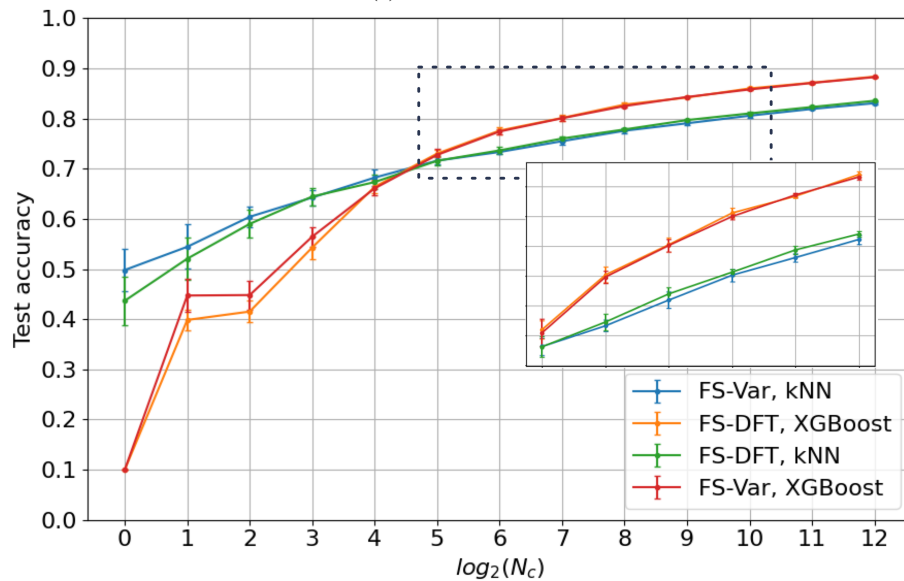
2.2 HOG-I and HOG-II

Based on the three modules introduced in Sec. 2.1, we propose two HOG-based learning systems below.

1. HOG-I
 - Objective: targeting at weaker supervision
 - Representation Learning: HOG features
 - Feature Learning: variance thresholding
 - Decision Learning: KNN
2. HOG-II



(a) MNIST Dataset



(b) Fashion-MNIST Dataset

Figure 2: Performance comparison of HOG-based learning systems on MNIST and Fashion-MNIST datasets under four different combinations among two feature learning methods (variance thresholding and DFT) and two classifiers (KNN and XGBoost) as a function of the training sample number per class in the log scale.

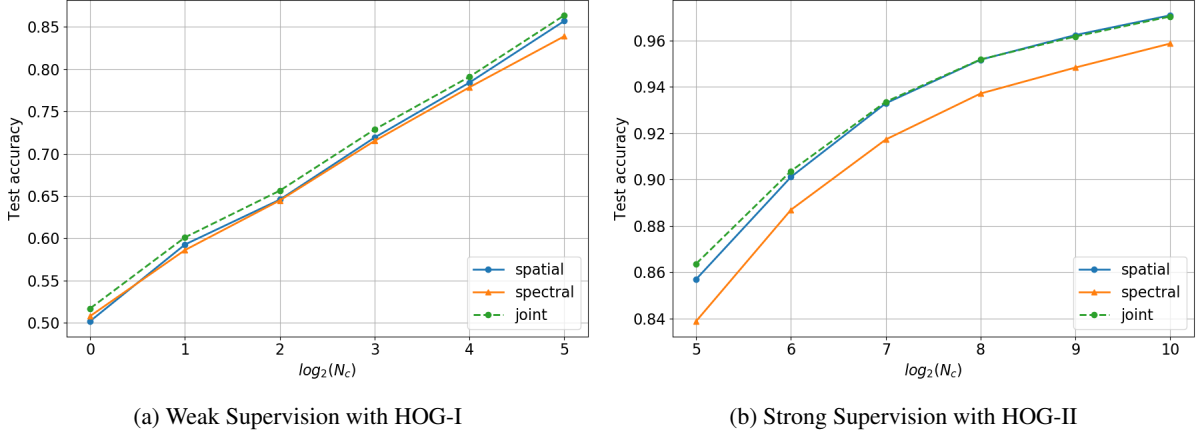


Figure 3: Performance comparison of spatial, spectral and joint HOG features on MNIST under weak and strong supervision conditions.

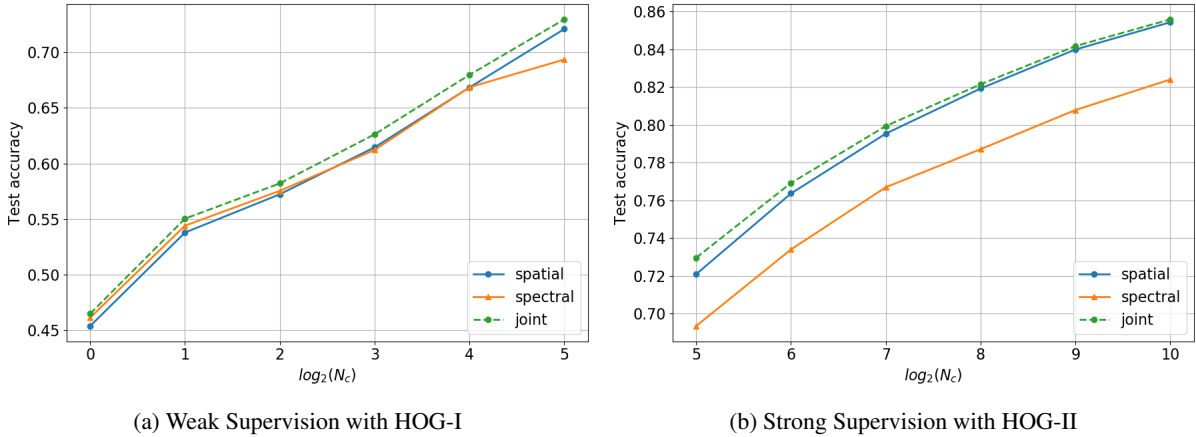


Figure 4: Performance comparison of spatial, spectral and joint HOG features on Fashion-MNIST under weak and strong supervision conditions.

- Objective: targeting at stronger supervision
- Representation Learning: HOG features
- Feature Learning: DFT
- Decision Learning: XGBoost

To justify these two designs, we conduct experiments on MNIST and Fashion-MNIST to gain more insights. By adopting the joint HOG features, we consider four combinations of two feature learning methods (variance thresholding and DFT) and two classifiers (KNN and XGBoost). The classification accuracy of test data against MNIST and Fashion-MNIST, as a function of the number of training data per class, N_c , is compared in Fig. 2, whose x-axis is in the unit of $\log_2 N_c = n_c$.

The primary factor to the performance is the classifier choice. When $N_c \leq 2^3 = 8$, the KNN classifier outperforms the XGBoost classifier by an obvious margin. If $N_c \geq 2^6 = 64$, the XGBoost classifier offers better performance. There is a cross over region between $N_c = 2^4 = 16$ and $N_c = 2^5 = 32$. Furthermore, by zooming into the weak supervision region with $N_c \leq 8$, the variance thresholding feature selection method is better than the DFT feature selection method. On the other hand, in the stronger supervision region with $N_c \geq 32$, the DFT feature selection method is better than the variance thresholding feature selection method. For this reason, we use the combination of variance thresholding and KNN in HOG-I and adopt the combination of DFT and XGBoost in HOG-II. They target at the weaker and stronger supervision cases, respectively.

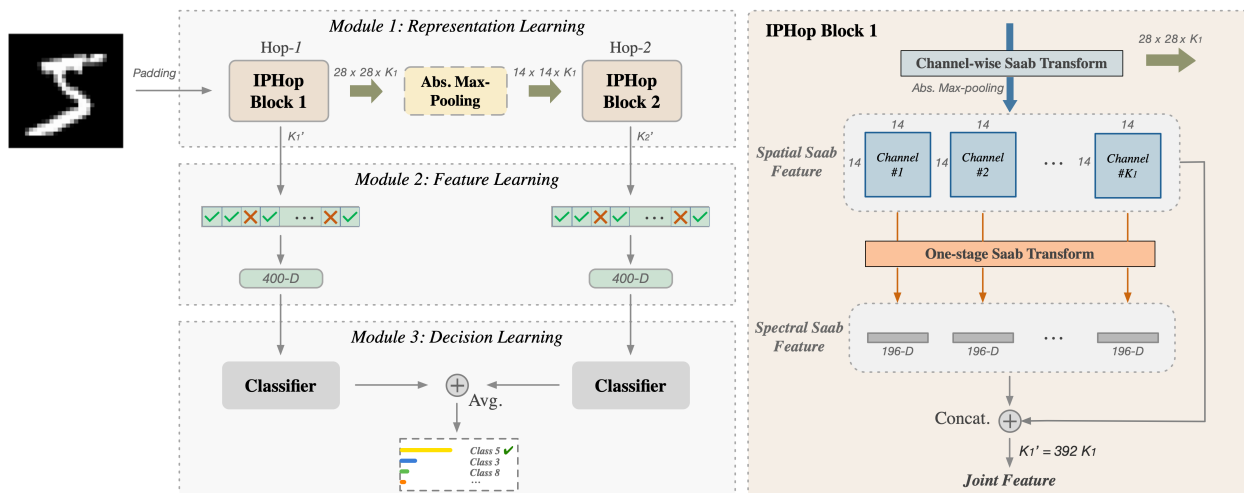


Figure 5: An overview of the SSL-based learning system, where the input image is of size 32×32 .

The phenomenon observed in Fig. 2 can be explained below. When the supervision degree is weak, it is difficult to build meaningful data models (e.g., low-dimensional manifolds in a high-dimensional representation space). Variance thresholding and KNN are classical feature selection and classification methods derived from the Euclidean distance, respectively. When the supervision degree becomes stronger, it is feasible to build more meaningful data models. The Euclidean distance measure is too simple to capture the data manifold information. Instead, DFT and XGBoost can leverage the manifold structure for better feature selection and decision making, respectively.

Next, we compare the performance of spatial, spectral and joint HOG features for HOG-I and HOG-II under their preferred supervision range for MNIST and Fashion-MNIST. Their results are shown in Figs. 3 and 4, respectively. We have the following observations. First, the performance gap between spatial and spectral HOG features is small under weak supervision with $2^4 = 16$ training samples per class. The performance gap becomes larger if the training sample number per class is greater or equal to $2^5 = 32$. Second, the joint HOG features provide the best overall performance. This is not a surprise since the set of joint HOG features contain the spatial and spectral HOG features as its two subsets. Here, we would like to point out that the performance gap between the joint HOG features and the spatial HOG features are larger for smaller N_c . It means that the spectral HOG features do complement the spatial HOG features and contribute to the performance gain. The value of spectral HOG features diminishes as N_c is sufficiently large.

We may give the following explanation to the phenomena observed in Figs. 3 and 4. By performing the DCT on the histogram of each bin over 8×8 patches, the values of low-frequency DCT coefficients are larger due to energy compaction. Their values for the same object class are relatively stable regardless of the supervision degree. In contrast, the spatial HOG features are distributed over the whole image. They are more sensitive to the local variation of each individual sample. Thus, when the supervision is weak, HOG-I can benefit from spectral HOG features. Second, as the supervision becomes stronger, the situation is different. Although the HOG of a single patch provides only the local information, we can obtain both local and global information by concatenating spatial HOG features across all patches. The HOG of at the same patch location could be noisy (i.e. varying from one sample to the other). Yet, the variation can be filtered out by DFT and XGBoost. On the other hand, the values of high-frequency DCT coefficients are small and many of them are close to zero because of energy compaction. Thus, spectral HOG features are not as discriminant as spatial HOG features under strong supervision.

3 Design of Learning Systems with SSL Features

Successive subspace learning (SSL) was recently introduced in [19, 20, 21, 22]. The technique has been applied to many applications such as point cloud classification, segmentation and registration [23, 24, 25, 26, 27], face recognition [28, 29], deepfake detection [30], anomaly detection [31], etc. SSL-based object classification work can be found in [32, 33, 34]. We propose two improved PixelHop learning systems and name them IPHop-I and IPHop-II in this section.

The system diagram of IPHop-I/II is shown in the left subfigure of Fig. 5. It consists of three modules: 1) unsupervised representation learning based on SSL features, 2) semi-supervised feature learning, and 3) supervised decision learning. Since its modules 2 and 3 are basically the same as those in HOG-based learning systems, we will primarily focus on

the representation learning in Sec. 3.1. Afterwards, we compare the performance of IPHop-I and IPHop-II under weak and strong supervision scenarios in Sec. 3.2.

3.1 SSL-based Representation Learning

We describe the processing procedure in Module 1 of the left subfigure of Fig. 5 below. The input is a tiny image of spatial resolution 32×32 . The processing procedure can be decomposed into two cascaded units, called Hop-1 and Hop-2, respectively. We first extract the spatial Saab features at Hop-1 and Hop-2. For each hop unit, we apply filters of spatial size 5×5 . At Hop-1, a neighborhood of size 5×5 centered at each of the interior 28×28 pixels is constructed. The Saab transform is conducted at each neighborhood to yield $K_1 = 25$ channel responses at each pixel. Afterwards, a 2×2 absolute max-pooling is applied to each channel. It reduces the spatial resolution from 28×28 to 14×14 . As a result, the input to Hop-2 is $14 \times 14 \times 25$. Similarly, we apply the channel-wise Saab transform with K_2 filters to the interior 10×10 points to get K_2 responses for each point. Here, we set $K_2 = 256$ and $K_2 = 204$ for MNIST and Fashion-MNIST, respectively, based on the energy thresholding criterion introduced in [33].

This above design is basically the standard PixelHop++ pipeline as described in [33]. The only modification in IPHop is that we change max-pooling in PixelHop++ to absolute max-pooling. Note that The responses from Hop-1 can be either positive or negative since no nonlinear activation is implemented at Hop-1. Instead of clipping negative values to zero, we find that it is advantageous to take the absolute value of the response first and then conduct the maximum pooling operation.

The spatial filter responses extracted at Hop-1 and Hop-2 only have a local view on the object due to the limited receptive field. They are not discriminant enough for semantic-level understanding. Since there exists correlations among these local filter responses, we can conduct another Saab transform across all local responses at each individual channel. Such a processing step provides the global spectral Saab features at Hop-1 and Hop-2 as shown in the right subfigure of Fig. 5. To explain the procedure in detail, we use Hop-1 as an example. For each of the $K_1 = 25$ channels, $14 \times 14 = 196$ spatial Saab features are flattened and then passed through a one-stage Saab transform. All responses are kept without truncation. Thus, the dimension of the output spectral Saab features is 196 for each channel. As compared to features learned by gradually enlarging the neighborhood range, the spectral Saab features capture the long range information from a finer scale. Finally, the spatial and spectral Saab features are concatenated at Hop-1 and Hop-2 to form the joint-spatial-spectral Saab features.

3.2 IPHop-I and IPHop-II

Since the two hops have different combinations of spatial and spectral information, it is desired to treat them differently. For this reason, we partition IPHop features into two sets:

- Feature Set no. 1: spatial and spectral features of Hop-1,
- Feature Set no. 2: spatial and spectral features of Hop-2.

Feature learning is used to select the subset of discriminant features from the raw representation. By following HOG-I and HOG-II, we consider variance thresholding and DFT two choices, apply them to feature sets no. 1 and no. 2, and select the same number of optimal features from each set individually. Furthermore, the same two classifiers are used for decision learning: KNN and XGBoost. For KNN, we concatenate optimal features from feature set no. 1 and no. 2, and compute the distance in this joint feature space. For XGBoost, we apply it to feature set no. 1 and no. 2 and make soft decision for each hop separately. Afterwards, we average the two soft decisions and use the maximum likelihood principle to yield the final decision.

We propose two SSL-based learning systems below.

1. IPHop-I

- Objective: targeting at weaker supervision
- Representation Learning: Joint SSL features (i.e. both feature set nos. 1 and 2)
- Feature Learning: variance thresholding
- Decision Learning: KNN

2. IPHop-II

- Objective: targeting at stronger supervision
- Representation Learning: Joint SSL features (i.e. both feature set nos. 1 and 2)
- Feature Learning: DFT

- Decision Learning: XGBoost

To justify these two designs, we consider all four possible combinations of feature and decision learning choices and compare their performance in Fig. 6. We use the fashion-MNIST dataset as an example in the following discussion. We see from Fig. 6(b) that KNN outperforms XGBoost under weak supervision (i.e. the training sample number per class $N_c \leq 4$). On the other hand, XGBoost outperforms KNN under stronger supervision ($N_c \geq 16$). There is a transition point at $N_c = 8$. For the weak supervision scenario, variance thresholding feature selection is better than DFT. This is particularly obvious when $N_c = 1$. The performance gap is around 25%. Thus, we use the combination of variance thresholding and KNN in IPHop-I to be used for weaker supervision. For the stronger supervision case, DFT is slightly better than variance thresholding in both KNN and XGBoost. Therefore, we use the combination of DFT and XGBoost in IPHop-II to be used for stronger supervision.

Next, we conduct ablation study on different representations for IPHop-I and IPHop-II in their preferred operating ranges to understand the impact of each feature type. Fig. 7 compares the test accuracy with individual spatial and spectral features of hop-1 and hop-2 and jointly for MNIST under different supervision levels.

Under weak supervision, we see from Fig. 7(a) that spectral features are more powerful than spatial features while spectral features of hop-2 are slightly better than those of hop-1. Under stronger supervision, we see from Fig. 7(b) that spatial features are more powerful than spectral features since spatial features can capture more detail information without energy compaction and the detail information does help the classification performance as the number of labeled sample increases. Furthermore, features of hop-2 are more useful than those of hop-1. The main differences between hop-1 and hop-2 features lie two factors:

- spatial features are determined by the receptive field of Saab filters,
- spectral features are determined by spatial aggregation of Saab responses over the entire set of grid points.

For the former, the cascaded filters in hop-2 offer a larger receptive field which has stronger discriminant power than hop-1. For the latter, hop-1 has 28x28 grid points while hop-2 has only 14x14 grid points. The content in hop-1 has larger diversity than that in hop-2. Although the spatial Saab transform can achieve energy compaction, the percentages of stable and discriminant spectral features in hop-1 tend to be fewer than those in hop-2. Yet, hop-1 and hop-2 do provide complementary features so that the joint feature set gives the best performance.

Finally, we show the test accuracy with individual spatial and spectral features of hop-1 and hop-2 and joint feature sets under different supervision levels for Fashion-MNIST in Fig. 8. The same observations and discussion apply to Fashion-MNIST.

4 Experiments

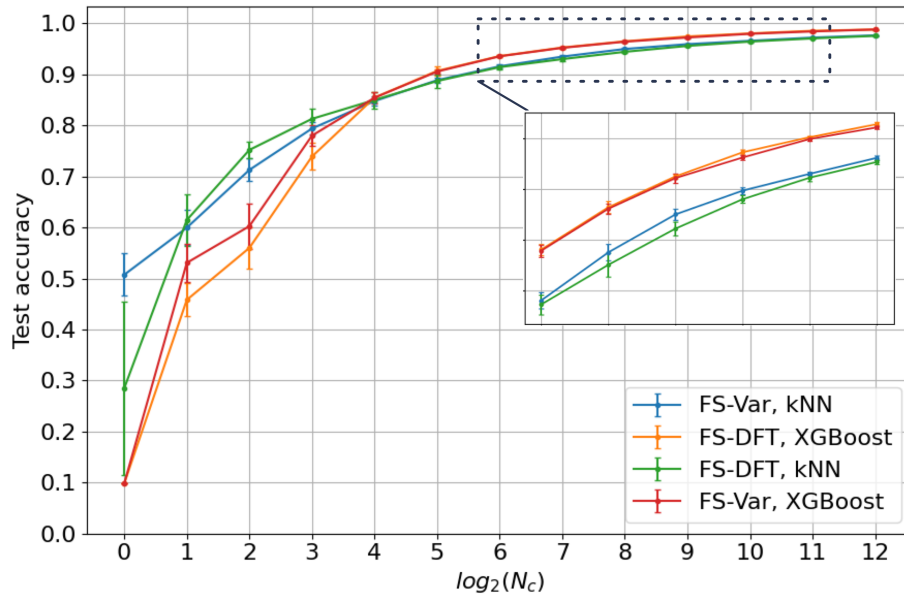
Experiments are conducted on MNIST [35] and Fashion-MNIST [36] datasets for performance benchmarking of HOG-I/II, IPHop-I/II and LeNet-5 learning systems against a wide range of supervision levels. For HOG and IPHop, we also introduce a hybrid solution. That is, type I is used when $N_c \leq 8$ while type II is used for $N_c \geq 16$. They are called hybrid HOG and hybrid IPHop, respectively.

4.1 Experimental Setup

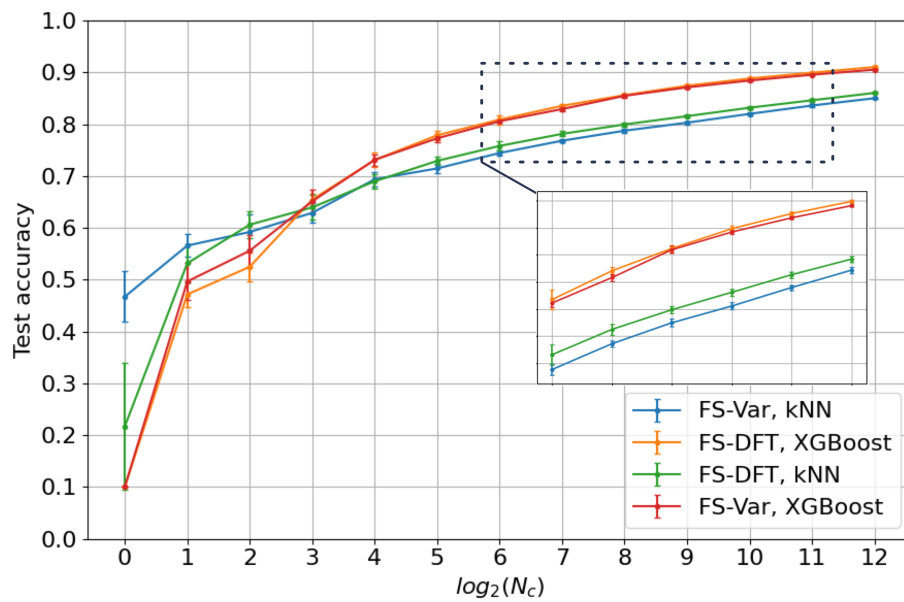
The Adam optimizer is used for backpropagation in the training of LeNet-5 network. The number of epochs is set to 50 for all N_c values. Both MNIST and Fashion-MNIST contain grayscale images of resolution 28×28 , with 60K training and 10K test images. MNIST contains 10 hand-written digits (from 0 to 9) in MNIST while Fashion-MNIST has 10 fashion classes. The training sample number per class is around 6K. Among the 6K training samples per class, we choose its subset of size $N_c = 2^{n_c}$, $n_c = 0, 1, \dots, 12$ randomly as the training set. All classes have the same training sample number. In words, we go from the extremely weak supervision condition with 1 labeled sample per class to the strong supervision condition with 4,096 labeled sample per class with gradual transition in between. Experiments with random training sample selection are performed with multiple runs. The dimension of representations and features for HOG and IPHop learning systems are summarized in Table 1 and Table 2, respectively.

4.2 Performance Benchmarking

We conduct performance benchmarking of HOG-I, HOG-II, IPHop-I, IPHop-II, and LeNet-5 in this subsection. The mean test accuracy and standard deviation values for MNIST and Fashion-MNIST under different supervision levels are reported in Table 3 and Table 4, respectively, based on results from 10 runs. We have the following observations.



(a) MNIST Dataset



(b) Fashion-MNIST Dataset

Figure 6: Performance comparison of SSL-based learning systems on MNIST and Fashion-MNIST datasets under four different combinations among two feature learning methods (variance thresholding and DFT) and two classifiers (KNN and XGBoost) as a function of $n_c = \log_2(N_c)$.

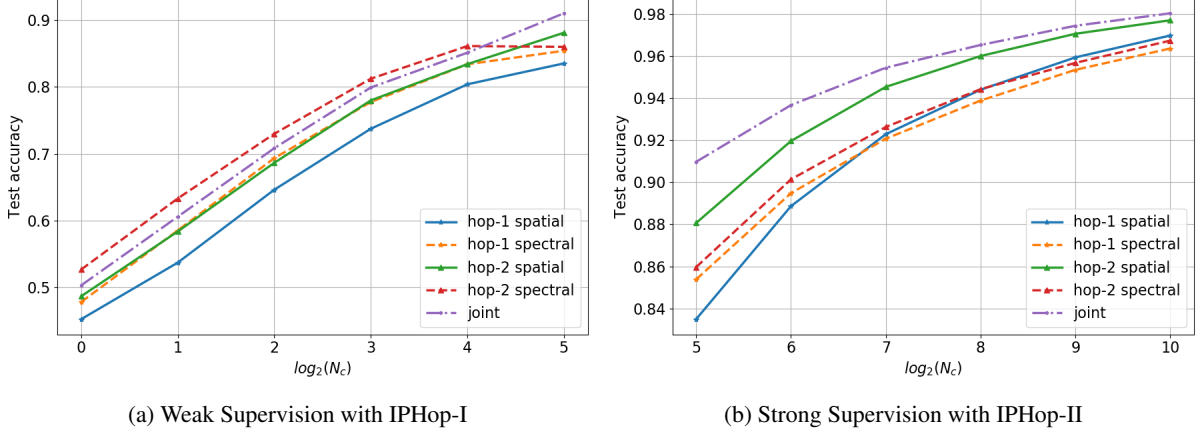


Figure 7: Performance comparison of spatial, spectral and joint SSL features on MNIST under strong and weak supervision conditions.

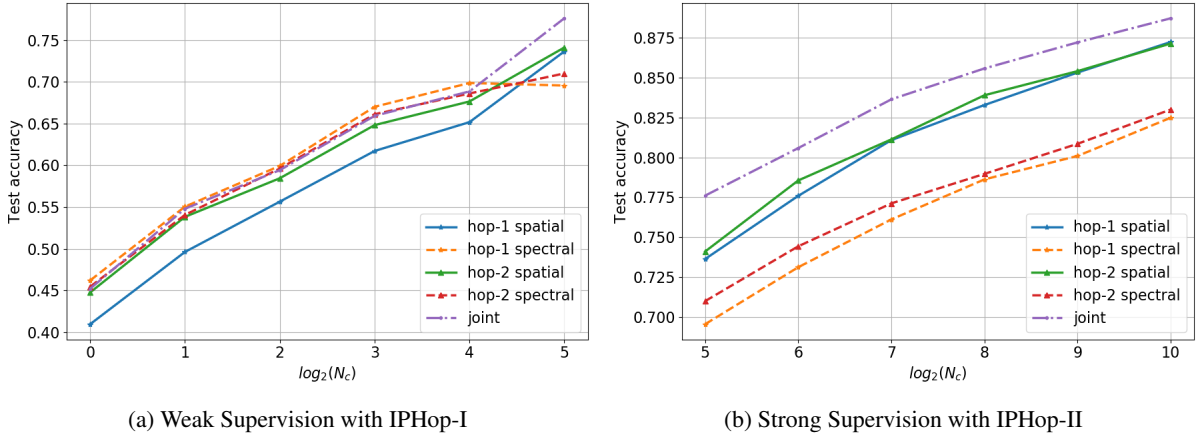


Figure 8: Performance comparison of spatial, spectral and joint SSL features on Fashion-MNIST under strong and weak supervision conditions.

- Under weak supervision with $N_c = 1, 2, 4, 8$, HOG-I and IPHop-I outperforms LeNet-5 by a large margin. Specifically, where there is only one labeled image per class ($N_c = 1$) or 10 labeled data for the whole dataset, HOG-I and IPHop-I can still reach an accuracy of around 50% on for both datasets. For MNIST, HOG-I and IPHop-I surpass LeNet-5 by 12.51% and 10.67%, respectively. For Fashion-MNIST, the performance gains of HOG-I and IPHop-I are 8.62% and 5.55%, respectively. It shows that the performance of HOG-based and IPHop learning systems is more robust as the number of labeled samples decreases.
- Under middle supervision with $N_c = 16, 32, 64, 128$, HOG-I, HOG-II, IPHop-I and IPHop-II still outperform LeNet-5. Furthermore, we start to see the advantage of HOG-II over HOG-I and the advantage of IPHop-II over IPHop-I. Besides comparison of mean accuracy scores, we see that the standard deviation of LeNet-5 is significantly higher than that of HOG-I, HOG-II, IPHop-I and IPHop-II under the weak and middle supervision levels.
- Under strong supervision with $N_c \geq 1,024$ (or the total training sample number is more than 10,240 since there are 10 classes), the advantage of LeNet-5 starts to show up. Yet, IPHop-II still outperforms LeNet-5 in Fashion-MNIST while the performance difference between IPHop-II and LeNet-5 on MNIST is very small.
- When the full training dataset (i.e., $N_c = 6K$) is used, each of HOG-I, HOG-II, IPHop-I and IPHop-II has a single test accuracy value and the standard deviation value is zero since the training set is the same. In contrast, even with the same input, LeNet-5 can yield different accuracy values due to the stochastic optimization nature of backpropagation.

Table 1: Summary of output dimensions of the HOG framework for MNIST and Fashion-MNIST.

| | | MNIST | Fashion-MNIST |
|----------|----------------------------|-------|---------------|
| Module-1 | Spatial HOG | 512 | 512 |
| | Spectral HOG | 512 | 512 |
| | Joint-Spatial-Spectral HOG | 1,024 | 1,024 |
| Module-2 | | 400 | 600 |

Table 2: Summary of output resolutions/dimensions of IPHop-II for MNIST and Fashion-MNIST.

| | | MNIST | | Fashion-MNIST | |
|----------|-----------------------------|----------------------------|---------------------------|----------------------------|---------------------------|
| | | Hop-1 | Hop-2 | Hop-1 | Hop-2 |
| Module-1 | Spatial Saab | $(14 \times 14) \times 25$ | $(5 \times 5) \times 256$ | $(14 \times 14) \times 25$ | $(5 \times 5) \times 204$ |
| | Spectral Saab | 196×25 | 25×256 | 196×25 | 25×204 |
| | Joint-Spatial-Spectral Saab | 9,800 | 12,800 | 9,800 | 10,200 |
| Module-2 | | 400 | 400 | 400 | 400 |

It is natural to consider hybrid HOG and IPHop schemes, where type I is adopted when $N_c \leq 8$ and type II is adopted for $N_c \geq 16$. For ease of visual comparison, we plot the mean accuracy curves as well as the standard deviation values (indicated by vertical bars) of hybrid HOG, hybrid IPHop and LeNet-5 as a function of N_c in Fig. 9. Clearly, hybrid IPHop provides the best overall performance among the three. Hybrid IPHop outperforms LeNet-5 by a significant margin when $N_c \leq 128$ on MNIST and throughout the whole range of N_c on Fashion-MNIST. As to hybrid HOG, it outperforms LeNet-5 with $N_c \leq 128$, underperforms LeNet-5 with $N_c \geq 512$ and has a crossover point with LeNet-5 at $N_c = 256$ on MNIST. Hybrid HOG has higher accuracy than LeNet-5 when $N_c \leq 1,024$ while its performance is comparable with LeNet-5 when $N_c = 2,048$ or $4,096$.

5 Discussion

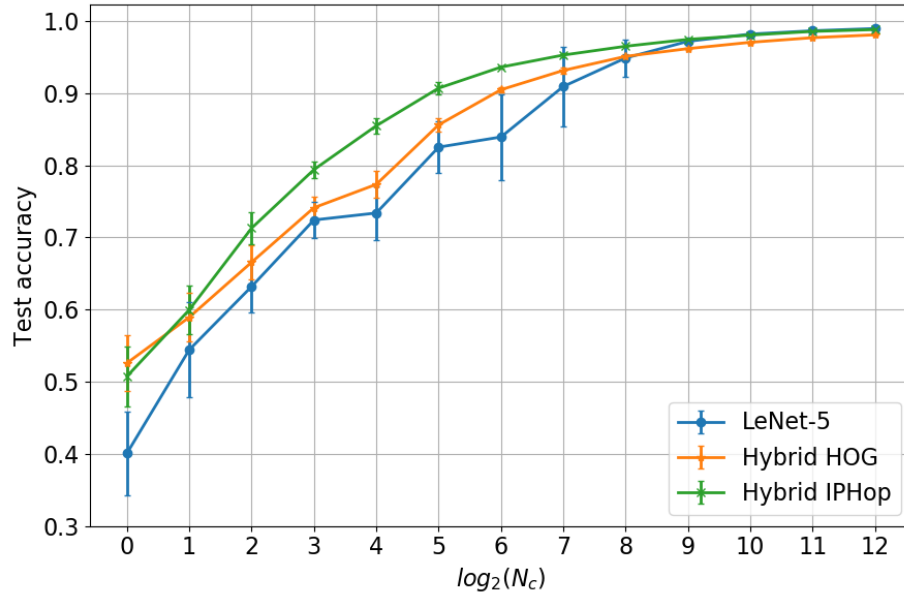
The superiority of hybrid IPHop under both weak and strong supervision conditions is clearly demonstrated in Fig. 9. We would like to provide some explanations in this section.

- Robustness in Representation Learning

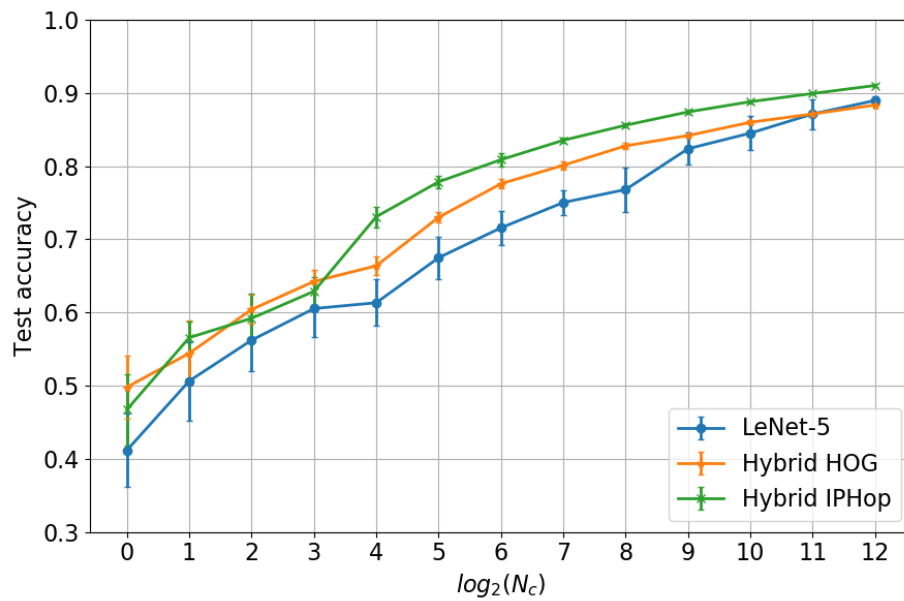
The IPHop representation is determined by Saab filters. Saab filters are obtained by PCA, which is an eigen-analysis of the covariance matrix of input vectors. If the covariance matrix converges fast as the training sample number increases, then IPHop’s feature learning is robust with respect to supervision degree. We show the Frobenius norm of the difference matrix between the covariance matrix derived by N_c training images and the full training size in Fig. 10. There are four cases; namely, the local and global Saab filters in Hop-1 and Hop-2, respectively. The results are averaged among 5 runs. We see that the Frobenius norm of the difference covariance matrices is already small even for $N_c = 1$. This is because one image contains many small patches which contribute to a robust covariance matrix.

Table 3: Comparison of the mean test accuracy (%) and standard deviation on MNIST under weak, middle and strong Supervision degree, where the best performance is highlighted in bold.

| Supervision | N_c | LeNet-5 | HOG-I | HOG-II | IPHop-I | IPHop-II |
|-------------|-------|-----------------------------|-----------------------------|----------------------|-----------------------------|-----------------------------|
| Weak | 1 | 40.07 (± 5.78) | 52.58 (± 3.89) | 9.80 (± 0.00) | 50.74 (± 4.13) | 9.80 (± 0.00) |
| | 2 | 54.43 (± 6.62) | 58.94 (± 3.33) | 38.40 (± 2.14) | 59.96 (± 3.42) | 45.82 (± 3.23) |
| | 4 | 63.19 (± 3.52) | 66.55 (± 2.42) | 43.48 (± 4.18) | 71.28 (± 2.22) | 56.00 (± 3.98) |
| | 8 | 72.41 (± 2.50) | 74.12 (± 1.50) | 63.39 (± 3.21) | 79.40 (± 1.18) | 73.90 (± 2.62) |
| Middle | 16 | 73.38 (± 3.69) | 78.61 (± 1.04) | 77.35 (± 1.80) | 84.78 (± 0.87) | 85.47 (± 1.02) |
| | 32 | 82.51 (± 3.62) | 82.87 (± 0.40) | 85.60 (± 0.99) | 88.87 (± 0.44) | 90.69 (± 0.85) |
| | 64 | 83.92 (± 5.94) | 86.01 (± 0.72) | 90.47 (± 0.34) | 91.60 (± 0.32) | 93.60 (± 0.21) |
| | 128 | 90.92 (± 5.52) | 88.34 (± 0.30) | 93.14 (± 0.43) | 93.49 (± 0.32) | 95.27 (± 0.24) |
| Strong | 256 | 94.87 (± 2.61) | 90.29 (± 0.23) | 95.09 (± 0.26) | 94.99 (± 0.23) | 96.49 (± 0.08) |
| | 512 | 97.17 (± 0.26) | 91.77 (± 0.20) | 96.16 (± 0.15) | 95.93 (± 0.14) | 97.44 (± 0.09) |
| | 1024 | 98.18 (± 0.16) | 93.02 (± 0.12) | 97.04 (± 0.14) | 96.59 (± 0.08) | 98.04 (± 0.07) |
| | 2048 | 98.64 (± 0.17) | 93.95 (± 0.12) | 97.68 (± 0.04) | 97.23 (± 0.08) | 98.55 (± 0.07) |
| | 4096 | 98.95 (± 0.09) | 94.70 (± 0.13) | 98.08 (± 0.04) | 97.66 (± 0.06) | 98.90 (± 0.06) |
| | Full | 99.07 (± 0.07) | 95.03 | 98.20 | 98.08 | 99.04 |



(a) MNIST



(b) Fashion-MNIST

Figure 9: Comparison of test accuracy between hybrid HOG, hybrid IPHop, and LeNet-5 for MNIST and Fashion-MNIST. For hybrid HOG and IPHop, type I is adopted when $N_c \leq 8$ and type II is adopted for $N_c \geq 16$.

Table 4: Comparison of the mean test accuracy (%) and standard deviation on Fashion-MNIST under weak, middle and strong Supervision degree, where the best performance is highlighted in bold.

| Supervision | N_c | LeNet-5 | HOG-I | HOG-II | IPHop-I | IPHop-II |
|-------------|------|----------------------|-----------------------------|----------------------|-----------------------------|-----------------------------|
| Weak | 1 | 41.18 (± 5.06) | 49.80 (± 4.29) | 10.00 (± 0.00) | 46.73 (± 4.87) | 10.00 (± 0.00) |
| | 2 | 50.65 (± 5.36) | 54.43 (± 4.42) | 39.85 (± 2.07) | 56.57 (± 2.16) | 47.17 (± 2.42) |
| | 4 | 56.22 (± 4.23) | 60.42 (± 1.99) | 41.53 (± 2.21) | 59.21 (± 3.39) | 52.48 (± 2.73) |
| | 8 | 60.54 (± 3.85) | 64.25 (± 1.58) | 54.29 (± 2.28) | 62.90 (± 1.91) | 65.44 (± 1.10) |
| Middle | 16 | 61.34 (± 3.17) | 68.22 (± 1.71) | 66.38 (± 1.33) | 69.37 (± 1.47) | 73.93 (± 1.41) |
| | 32 | 67.49 (± 2.88) | 71.60 (± 0.75) | 73.02 (± 0.74) | 71.47 (± 0.89) | 77.86 (± 0.88) |
| | 64 | 71.58 (± 2.33) | 73.33 (± 0.48) | 77.60 (± 0.66) | 74.44 (± 0.52) | 80.88 (± 0.89) |
| | 128 | 75.04 (± 1.65) | 75.49 (± 0.68) | 80.12 (± 0.57) | 76.81 (± 0.28) | 83.54 (± 0.37) |
| Strong | 256 | 76.81 (± 3.05) | 77.57 (± 0.52) | 82.78 (± 0.41) | 78.74 (± 0.37) | 85.59 (± 0.33) |
| | 512 | 82.38 (± 2.19) | 79.05 (± 0.37) | 84.19 (± 0.17) | 80.29 (± 0.31) | 87.41 (± 0.25) |
| | 1024 | 84.51 (± 2.34) | 80.56 (± 0.38) | 86.00 (± 0.25) | 81.99 (± 0.26) | 88.81 (± 0.20) |
| | 2048 | 87.13 (± 2.06) | 81.91 (± 0.24) | 87.14 (± 0.17) | 83.59 (± 0.26) | 89.93 (± 0.13) |
| | 4096 | 88.97 (± 0.56) | 83.06 (± 0.18) | 88.35 (± 0.08) | 85.01 (± 0.11) | 91.03 (± 0.16) |
| | Full | 89.54 (± 0.33) | 83.52 | 88.84 | 85.77 | 91.37 |

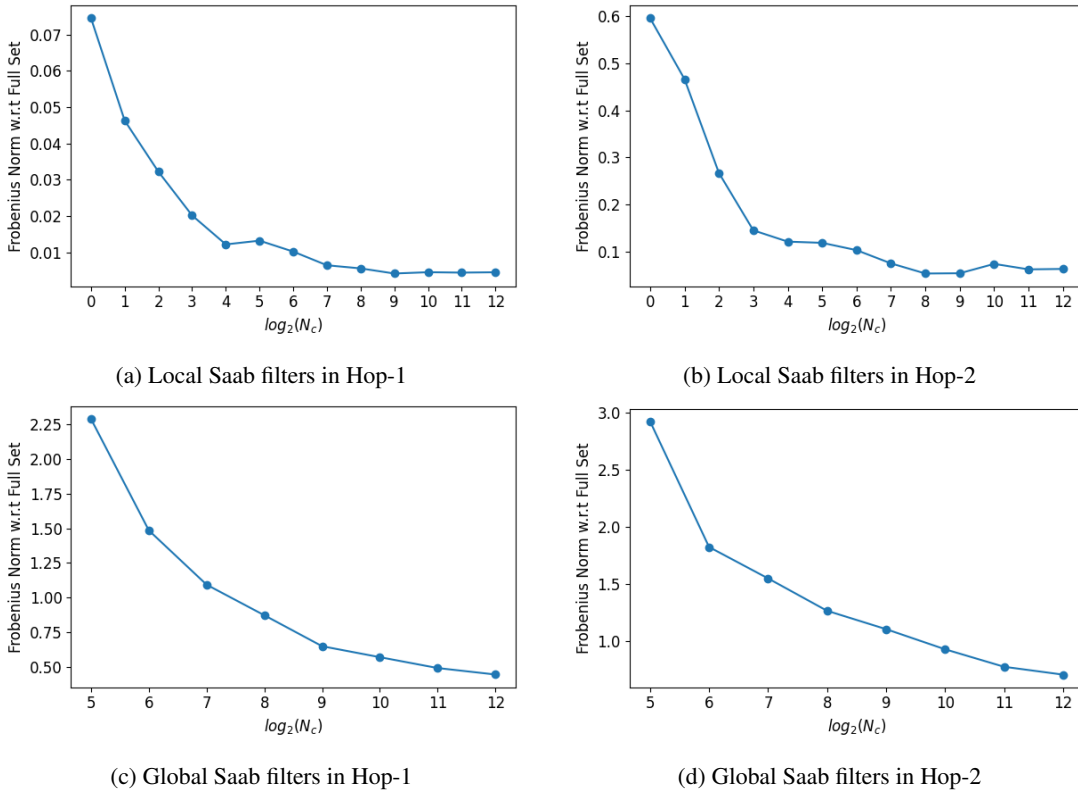


Figure 10: The plot of Frobenius norms of difference matrices between the covariance matrices learned under different supervision levels and the one learned from the full set for MNIST.

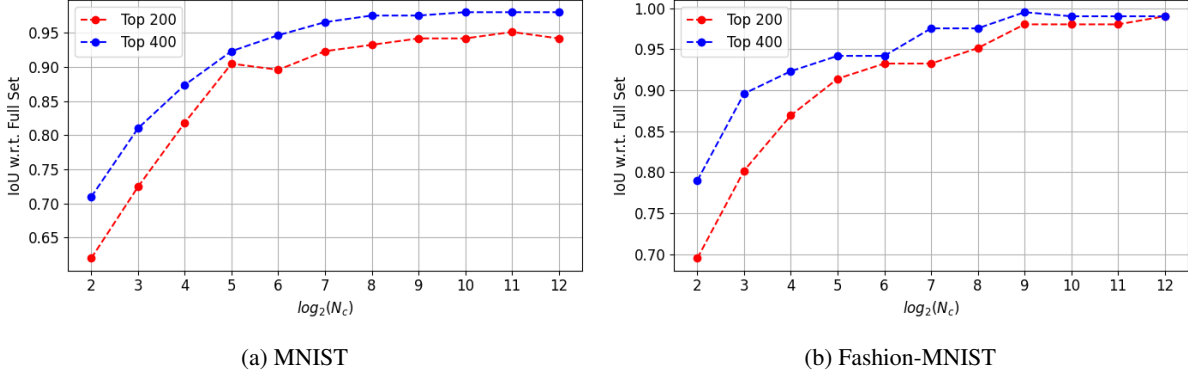


Figure 11: IoU scores between the feature sets selected using full training size and using N_c on MNIST and Fashion-MNIST.

- Robustness in Feature Learning

To demonstrate the robustness of DFT, we measure the overlapping of the selected feature set based on N_c training samples and that based on the full training size ($N_c = 6K$). These two sets are denoted by $\{F\}_{N_c}$ and $\{F\}_{full}$, respectively. We define an intersection-over-union (IoU) score as

$$IoU_{N_c} = \frac{|\{F\}_{full} \cap \{F\}_{N_c}|}{|\{F\}_{full} \cup \{F\}_{N_c}|}, \quad (3)$$

where the numerator represents for the number of features agreed between the two subsets while the denominator represents the number of features selected by at least one of the two subsets. For each N_c , there exists randomness in selecting a subsets of labeled samples. To eliminate the randomness, we calculate the averaged IoU values with 10 runs. The IoU values of selecting the top 200-D and 400-D from the 1024-D HOG features for MNIST and Fashion-MNIST, respectively, are shown in Fig. 11. We see that, as the number of labeled data increases, the IoU score increases. With a small N_c value (say, 32) the IoU score can already reach 90%. It clearly shows that DFT is a semi-supervised feature selection tool and it can work well under very weak supervision condition.

- Robustness in Decision Learning

The KNN classifier is used when the training number is small. It is an exemplar-based classifier. Instead of minimizing the loss using labeled data, it finds the most similar training sample based on the Euclidean distance in the feature space. However, it cannot capture the data manifold that often lies in a higher dimensional feature space. As the number of labeled data increases, XGBoost is more powerful. It minimizes the cross-entropy loss with a gradient boosting technique. XGBoost is a decision tool based on ensemble learning which explains its robust decision behavior.

On the other hand, it is desired to understand the behaviour of LeNet-5 under different supervision levels. We show the learning curves of LeNet-5 on MNIST using $N_c = 2^{n_c}$, $n_c = 0, 1, \dots, 12$, in Fig. 12, which are expressed as the cross-entropy loss as a function of the epoch number. The batch size in each epoch is set to the total number of labeled images if $N_c \leq 16$ and 128 if $N_c > 16$. The loss curves are averaged among 5 random runs. The loss decreases slowly and converges at a higher loss value when N_c is small. In contrast, it decreases faster and converges at a lower loss value when N_c is larger. Clearly, the learning performance of LeNet-5 in both convergence rates and converged loss values is highly dependent on the number of the labeled samples.

6 Conclusion and Future Work

In this work, we compared the supervision-scalability of three learning systems; namely, the HOG-based and IPHop-based learning systems and LeNet-5, which is an representative deep-learning system. Both HOG-based and IPHop-based learning systems work better than LeNet-5 under weak supervision. As the supervision degree goes higher, the performance gap narrows. Yet, IPHop-II still outperforms LeNet-5 on Fashion-MNIST under strong supervision.

It is well known that it is essential to have a sufficient amount of labeled data for deep learning systems to work properly. Data augmentation and adoption of pre-trained networks are two commonly used techniques to overcome the problem of insufficient training data at the cost of larger model sizes and higher computational cost. Our performance

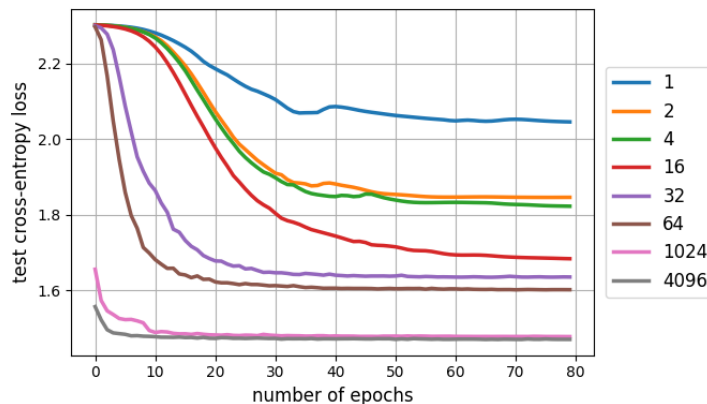


Figure 12: Learning curve using LeNet-5 on MNIST dataset with selected supervision levels.

benchmarking study is only preliminary. In the future, we would like to conduct further investigation by considering supervision scalability, tradeoff of accuracy, model sizes and computational complexity jointly.

Acknowledgement

The authors acknowledge the Center for Advanced Research Computing (CARC) at the University of Southern California for providing computing resources that have contributed to the research results reported within this publication.

References

- [1] J. Foulds and E. Frank, “A review of multi-instance learning assumptions,” *The knowledge engineering review*, vol. 25, no. 1, pp. 1–25, 2010.
- [2] X.-S. Wei, J. Wu, and Z.-H. Zhou, “Scalable algorithms for multi-instance learning,” *IEEE transactions on neural networks and learning systems*, vol. 28, no. 4, pp. 975–987, 2016.
- [3] D. Angluin and P. Laird, “Learning from noisy examples,” *Machine Learning*, vol. 2, no. 4, pp. 343–370, 1988.
- [4] B. Fréney and M. Verleysen, “Classification in the presence of label noise: a survey,” *IEEE transactions on neural networks and learning systems*, vol. 25, no. 5, pp. 845–869, 2013.
- [5] Z.-H. Zhou, “A brief introduction to weakly supervised learning,” *National science review*, vol. 5, no. 1, pp. 44–53, 2018.
- [6] Z.-Y. Zhang, P. Zhao, Y. Jiang, and Z.-H. Zhou, “Learning from incomplete and inaccurate supervision,” *IEEE Transactions on Knowledge and Data Engineering*, 2021.
- [7] O. Chapelle, B. Scholkopf, and A. Zien, “Semi-supervised learning (chappelle, o. et al., eds.; 2006)[book reviews],” *IEEE Transactions on Neural Networks*, vol. 20, no. 3, pp. 542–542, 2009.
- [8] X. Zhu and A. B. Goldberg, “Introduction to semi-supervised learning,” *Synthesis lectures on artificial intelligence and machine learning*, vol. 3, no. 1, pp. 1–130, 2009.
- [9] Z.-H. Zhou and M. Li, “Semi-supervised learning by disagreement,” *Knowledge and Information Systems*, vol. 24, no. 3, pp. 415–439, 2010.
- [10] J. E. Van Engelen and H. H. Hoos, “A survey on semi-supervised learning,” *Machine Learning*, vol. 109, no. 2, pp. 373–440, 2020.
- [11] B. Settles, “Active learning literature survey,” 2009.
- [12] E. Haussmann, M. Fenzi, K. Chitta, J. Ivanecy, H. Xu, D. Roy, A. Mittel, N. Koumchatzky, C. Farabet, and J. M. Alvarez, “Scalable active learning for object detection,” in *2020 IEEE intelligent vehicles symposium (iv)*, pp. 1430–1435, IEEE, 2020.
- [13] M. Fink, “Object classification from a single example utilizing class relevance metrics,” *Advances in neural information processing systems*, vol. 17, 2004.

- [14] Q. Sun, Y. Liu, T.-S. Chua, and B. Schiele, “Meta-transfer learning for few-shot learning,” in *Proceedings of the IEEE/CVF Conference on Computer Vision and Pattern Recognition*, pp. 403–412, 2019.
- [15] Y. Chen, Z. Liu, H. Xu, T. Darrell, and X. Wang, “Meta-baseline: exploring simple meta-learning for few-shot learning,” in *Proceedings of the IEEE/CVF International Conference on Computer Vision*, pp. 9062–9071, 2021.
- [16] N. Dalal and B. Triggs, “Histograms of oriented gradients for human detection,” in *2005 IEEE computer society conference on computer vision and pattern recognition (CVPR’05)*, vol. 1, pp. 886–893, Ieee, 2005.
- [17] Y. Yang, W. Wang, H. Fu, and C.-C. J. Kuo, “On supervised feature selection from high dimensional feature spaces,” *arXiv preprint arXiv:2203.11924*, 2022.
- [18] T. Chen, T. He, M. Benesty, V. Khotilovich, Y. Tang, H. Cho, K. Chen, *et al.*, “Xgboost: extreme gradient boosting,” *R package version 0.4-2*, vol. 1, no. 4, pp. 1–4, 2015.
- [19] C.-C. J. Kuo, “Understanding convolutional neural networks with a mathematical model,” *Journal of Visual Communication and Image Representation*, vol. 41, pp. 406–413, 2016.
- [20] C.-C. J. Kuo, “The cnn as a guided multilayer recos transform [lecture notes],” *IEEE signal processing magazine*, vol. 34, no. 3, pp. 81–89, 2017.
- [21] C.-C. J. Kuo and Y. Chen, “On data-driven saak transform,” *Journal of Visual Communication and Image Representation*, vol. 50, pp. 237–246, 2018.
- [22] C.-C. J. Kuo, M. Zhang, S. Li, J. Duan, and Y. Chen, “Interpretable convolutional neural networks via feedforward design,” *Journal of Visual Communication and Image Representation*, 2019.
- [23] M. Zhang, H. You, P. Kadam, S. Liu, and C.-C. J. Kuo, “Pointhop: An explainable machine learning method for point cloud classification,” *IEEE Transactions on Multimedia*, 2020.
- [24] M. Zhang, Y. Wang, P. Kadam, S. Liu, and C.-C. J. Kuo, “Pointhop++: A lightweight learning model on point sets for 3d classification,” in *2020 IEEE International Conference on Image Processing (ICIP)*, pp. 3319–3323, IEEE, 2020.
- [25] M. Zhang, P. Kadam, S. Liu, and C.-C. J. Kuo, “Unsupervised feedforward feature (uff) learning for point cloud classification and segmentation,” in *2020 IEEE International Conference on Visual Communications and Image Processing (VCIP)*, pp. 144–147, IEEE, 2020.
- [26] P. Kadam, M. Zhang, S. Liu, and C.-C. J. Kuo, “Unsupervised point cloud registration via salient points analysis (spa),” in *2020 IEEE International Conference on Visual Communications and Image Processing (VCIP)*, pp. 5–8, IEEE, 2020.
- [27] P. Kadam, M. Zhang, S. Liu, and C.-C. J. Kuo, “R-pointhop: A green, accurate, and unsupervised point cloud registration method,” *IEEE Transactions on Image Processing*, vol. 31, pp. 2710–2725, 2022.
- [28] M. Rouhsedaghat, Y. Wang, X. Ge, S. Hu, S. You, and C.-C. J. Kuo, “Facehop: A light-weight low-resolution face gender classification method,” *arXiv preprint arXiv:2007.09510*, 2020.
- [29] M. Rouhsedaghat, M. Monajatipoor, Z. Azizi, and C.-C. J. Kuo, “Successive subspace learning: An overview,” *arXiv preprint arXiv:2103.00121*, 2021.
- [30] H.-S. Chen, M. Rouhsedaghat, H. Ghani, S. Hu, S. You, and C.-C. J. Kuo, “Defakehop: A light-weight high-performance deepfake detector,” in *2021 IEEE International Conference on Multimedia and Expo (ICME)*, pp. 1–6, IEEE, 2021.
- [31] K. Zhang, B. Wang, W. Wang, F. Sohrab, M. Gabbouj, and C.-C. J. Kuo, “Anomalyhop: An ssl-based image anomaly localization method,” *arXiv preprint arXiv:2105.03797*, 2021.
- [32] Y. Chen and C.-C. J. Kuo, “Pixelhop: A successive subspace learning (ssl) method for object recognition,” *Journal of Visual Communication and Image Representation*, vol. 70, p. 102749, 2020.
- [33] Y. Chen, M. Rouhsedaghat, S. You, R. Rao, and C.-C. J. Kuo, “Pixelhop++: A small successive-subspace-learning-based (ssl-based) model for image classification,” in *2020 IEEE International Conference on Image Processing (ICIP)*, pp. 3294–3298, IEEE, 2020.
- [34] Y. Yang, V. Magoulianitis, and C. C. J. Kuo, “E-pixelhop: An enhanced pixelhop method for object classification,” *2021 Asia-Pacific Signal and Information Processing Association Annual Summit and Conference (APSIPA ASC)*, pp. 1475–1482, 2021.
- [35] Y. LeCun, L. Bottou, Y. Bengio, and P. Haffner, “Gradient-based learning applied to document recognition,” *Proceedings of the IEEE*, vol. 86, no. 11, pp. 2278–2324, 1998.
- [36] H. Xiao, K. Rasul, and R. Vollgraf, “Fashion-mnist: a novel image dataset for benchmarking machine learning algorithms,” *arXiv preprint arXiv:1708.07747*, 2017.